

# Cobalt Activates Oxygen Evolution

Much effort has been devoted to investigate electrochemically the ion of the oxygen-evolution reaction (OER) in pursuit of sustainable and efficient energy conversion and storage. The inherent sluggish kinetics of the four-electron transfer make OER a key step for energy-conversion and energy-storage devices including cells for water electrolysis and for photoelectrochemical splitting of water, and rechargeable metal-air batteries. To overcome this rate-limiting step, extensive research has been dedicated to develop efficient OER electrocatalysts with high activity and small overpotential. Recent reports of highly economic and efficient electrochemical catalysts have significantly advanced this technology, but the largest challenge concerning the reliability of the catalyst remains unconquered. A major reason for the slow progress of reliable catalysts in the OER is that the electrocatalyst bears most charge carriers during the harsh oxidation because the OER normally occurs under a large anodic potential. A highly stable electrocatalyst must effectively transfer charge carriers to the OER electrocatalyst/electrolyte interface but retain a sufficient amount of oxidized species during anodization. To shed light on such complicated surface reactions, a tool to allow the observation of the active phase of metal centers under anodization *in situ* was required.

The oxygen evolution activity of electrocatalysts depends strongly on corresponding surface structures and adsorption energies of intermediates on metal-oxide surfaces. In general, the surface structure can affect the activity of an electrocatalyst and surface states can be further altered on introducing foreign elements, which leads to a considerably decreased overpotential and therefore increased activity during the OER. In practical conditions, the reactions of OER involve only a several-nanometer region of the catalyst surface, and studies within this limited region *in situ* are essential and extremely challenging. Hao-Ming Chen (National Taiwan University), Hwo-Shuenn Sheu (NSRRC) and Ting-Shan Chan (NSRRC) developed cooperatively the measurement of synchrotron-based X-ray spectroscopy *in situ* at BL01C1 and BL01C2 to track the atomic-scale structural changes on the surface of an electrode during OER in liquid conditions. They employed a  $\text{Co}_3\text{O}_4$  nanocube underlaid with a thin CoO layer and Ni-Co oxide nanosheets as two kinds of OER electrocatalysts.<sup>1,2</sup> The development to study and to investigate the surface of

a catalyst *in situ* might provide a powerful means to elucidate fundamental processes in an OER catalyst and eventually lead to a novel design principle.

In Chen's first work, a single-crystal  $\text{Co}_3\text{O}_4$  nanocube underlaid with a thin CoO layer resulted in a high-performance and highly stable electrocatalyst for the oxygen evolution reaction.<sup>1</sup> The strategy was to incorporate a surface layer well adapted to the active phases of the catalytic metal centers to enhance the stability of the electrocatalysts. A grazing-angle X-ray diffraction approach *in situ* in a liquid environment was achieved to determine the atomic structure of the catalyst surface in ambient conditions, especially for gas evolution (high potential region). Figure 1 (a) depicts the current density as a function of applied voltage, and is color-coded together with diffracted intensities recorded using synchrotron light at energy 12 keV. At an early stage (before  $\text{O}_2$  evolution), the main reflexes were attributed to the fluorine-doped tin-oxide substrate and the spinel-type  $\text{Co}_3\text{O}_4$  phases. No CoO phase was observed, indicating that the CoO layer was too thin to diffract the light

source (a few atomic layers). At a higher voltage, accompanying the formation of  $\beta$ - $\text{CoOOH}$  on the surface of the electrode, the electrodes began to evolve oxygen gas in both alkaline and neutral conditions. This effect indicated that the CoO layer was converted into a more active phase with increasing applied potential. When the applied voltage was further increased, a new phase,  $\alpha$ - $\text{CoOOH}$ , was observed.

Both alkaline and neutral conditions demonstrated a similar phenomenon in which OER was strongly correlated with the formation of metal oxyhydroxide. This evidence was direct for the formation of metal oxyhydroxide during greater evolution oxygen gas in a liquid environment *in situ*. Notably, the CoO layer functioned as an adapting junction between the electrolyte and the catalyst to ease the strain in the nanocrystal substrates when the active phases were formed. As shown in Fig. 1 (b), when the applied potential was cycled between +2.0 and +0.1 V (versus RHE; reversible hydrogen electrode), the X-ray diffraction approach *in situ* showed that this junction layer altered its structure reversibly

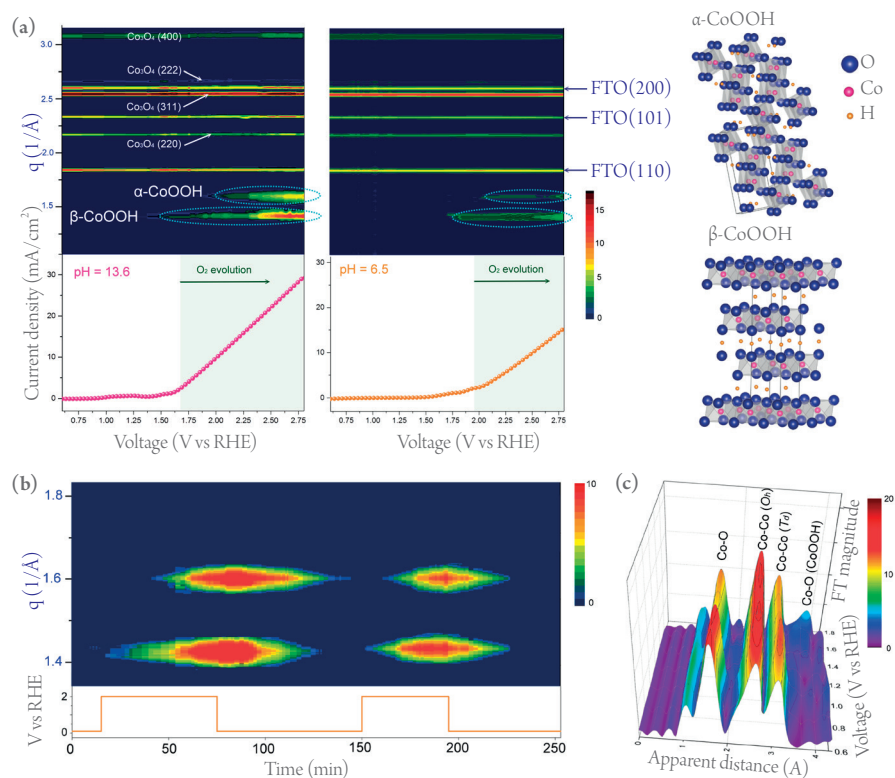


Fig. 1: (a) Contour plots of grazing-angle X-ray diffraction signals *in situ* of a  $\text{Co}_3\text{O}_4$ @CoO SC in an aqueous solution containing KOH and  $\text{Na}_2\text{SO}_4$ . The lower curves show the measured current density in both cases. (b) Contour plots of grazing-angle X-ray diffraction signals of a  $\text{Co}_3\text{O}_4$ @CoO SC in an alkaline aqueous solution *in situ* under switching of voltage (between 2.0 and 0.1 V versus RHE). (c) Voltage-dependent Fourier-transform EXAFS of a  $\text{Co}_3\text{O}_4$ @CoO single-crystal cube in an alkaline aqueous solution containing KOH and in a liquid cell *in situ*. [Reproduced from Ref. 1]

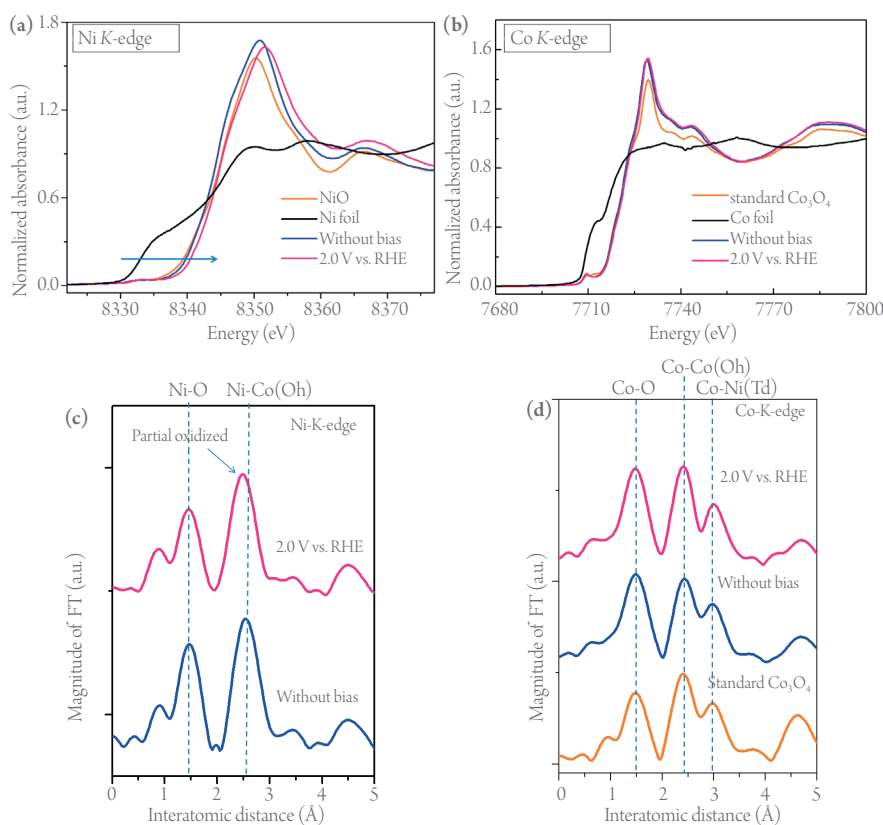


Fig. 2: Normalized (a) Ni K-edge and (b) Co K-edge XANES for NCO-HNS electrode *in situ* with and without an applied bias in NaOH solution (1 M). EXAFS oscillations extracted from (c) Ni K-edge and (d) Co K-edge EXAFS for NCO-HNS with and without applied bias *in situ* in NaOH solution (1 M). (e) Structural geometry model of NCO-HNS. [Reproduced from Ref. 2]

between metal oxyhydroxide and amorphous phases. This observation revealed that this skin junction adapted reversibly to the environment (applied potential) and the condition change during catalytic reaction, consequently protecting the underlying catalyst (for example,  $\text{Co}_3\text{O}_4$ ) anodizing from an applied bias.

Moreover, X-ray absorption in a liquid environment *in situ* with a small throughput current (below + 1.7 V versus RHE) was recorded; the extended X-ray absorption fine structure spectra (EXAFS) of  $\text{Co}_3\text{O}_4$ @CoO single-crystal cubes are depicted in Fig. 1(c). The first peak at 1.5 Å and the second and third peaks at 2.5 and 3.1 Å are assigned respectively to the single scattering paths of the closest oxygen (that is, Co-O) and the second/third neighboring cobalt metals (that is, Co-Co) surrounding the absorbing Co atoms. The Co-O distance (1.5 Å) is typical for a  $\text{Co}_3\text{O}_4$  normal spinel-type structure; the first Co-Co distance (2.5 Å) is typical for a Co (III)-Co bond with octahedrally coordinated Co atoms in a normal spinel structure. The second distance 3.1 Å is attributed to Co (II)-Co bonds with tetrahedrally coordinated Co atoms. These results are consistent with the results determined for the spinel structure of  $\text{Co}_3\text{O}_4$ . Notably, a new peak was observed at 3.8 Å when an increased potential + 1.7 V (versus RHE) was applied to a  $\text{Co}_3\text{O}_4$ @CoO

single-crystal cube electrode. The peak is attributed to the formation of a cobalt oxyhydroxide phase on the surface of the  $\text{Co}_3\text{O}_4$  single-crystal cubes, thus leading to a new scattering path of Co-O from the cobalt oxyhydroxide phase. The CoOOH layer formed from  $\text{Co}_3\text{O}_4$  nanocubes without covering the CoO skin was characteristic of a rough nature. Unlike  $\text{Co}_3\text{O}_4$  nanocubes, the CoOOH layer formed from  $\text{Co}_3\text{O}_4$  nanocubes with covering of the CoO skin exhibited a continuous and uniform surface. This observation is attributed to the presence of a CoO skin layer, whereas directly anodizing Co ions on a  $\text{Co}_3\text{O}_4$  nanocube surface resulted in a remarkably rough layer. A strong correlation existing between  $\text{O}_2$  gas evolution and the active metal centers with the oxyhydroxide phase was concluded using the voltage-dependent X-ray diffraction/absorption approach *in situ*. More importantly, this junction layer can reversibly adapt its structure to accommodate harsh conditions or an environment without breaking the underlying scaffold.

Another experiment was performed to construct Ni-Co oxide hierarchical nanosheets (NCO-HNS), delivering stable current density 10 mA  $\text{cm}^{-2}$  at overpotential 0.34 V for OER.<sup>2</sup> To realize the real active site for OER in the present Ni-Co hierarchical nanostructures, the oxidation states

of the NCO-HNS were monitored using X-ray-absorption near-edge structure (XANES) during oxidation *in situ* in alkaline media. The XANES of Ni K-edge spectra of the NCO-HNS electrode with and without applied bias in NaOH (1 M) is plotted in Fig. 2(a). The X-ray-absorption near-edge structure results exhibit a continuously increasing energy of the absorption edge from 8350.2 to 8350.7 eV during water oxidation, which is consistent with the general overall electrochemical scenario for the formation of NiOOH, resulting in a modification of the edge features related to the variation of the Ni-O local environment. The edge position shift (~ 0.5 eV) was accompanied with a considerably decreased intensity of the white line. This decrease of the white-line intensity of XANES indicated that the crystal evolved into a distorted octahedral structure upon oxidation. Co K-edge (~ 7729.3 eV) XANES of NCO-HNS *in situ* is shown in Fig. 2(b). Surprisingly, the X-ray-absorption near-edge structure spectra reveal that the features of the Co-K edge absorption spectra and the intensity of the white line were not obviously affected by the applied potential, indicating that Co remained as a mixture of Co(II)/Co(III) during the OER.

To realize further the roles of Ni and Co cations during OER, the EXAFS oscillations of a NCO-HNS electrode, as depicted in Figs. 2(c) and 2(d), were analyzed to clarify the local structural variations around the Ni and Co sites in the NCO-HNS structure. Interatomic distances were smaller because Fourier transform (FT) spectra were not phase-corrected. As shown in Fig. 2(c), the first peak at 1.5 Å and the second peak at 2.5 Å are attributed to the single scattering paths of Ni-O and the nearest-neighbor transition metals around absorbing Ni atoms, respectively. There was, notably, only one FT peak in a single scattering path from the nearest-neighbor transition metals, indicating that Ni cations were located in a tetrahedral site surrounded by coordinated oxygen. In contrast, as shown in Fig. 2(d), three FT peaks were present in EXAFS of the Co K-edge for a NCO-HNS electrode. In addition to the first peak at 1.5 Å from a single-scattering path of Co-O, the second peak at 2.5 Å and third FT peak at 3.0 Å result from the single-scattering path of nearest-neighbor transition metals around Co cations.

This phenomenon occurred because of the presence of a scattering transition metal around Co at two distances, indicating that Co cations were located in an octahedral site of coordinated oxygen, as the octahedrally coordinated cations had two bond

distances (interatomic distances) from a surrounding transition metal in an octahedral site and a tetrahedral site. Once a desired bias was applied at a NCO-HNS electrode, the second FT peak from single-scattering of Ni-Co path decreased relative to the unbiased condition (Fig. 2(c); Ni K-edge), which could be attributed to the partial oxidation of Ni cations, and further revealed the observation from X-ray-absorption near-edge structure of the Ni K-edge. In terms of Co cations, there was no considerable change with and without applied potential, which indicates that Ni cations acted as more active roles than Co cations in OER. Nevertheless, the role of Co on the surface of NCO-HNS during water oxidation cannot be totally excluded as a more active property of the Ni cation might result from a local environment generated by coordinated Co cations and oxygen anions. Furthermore, Co oxide might also act as a scaffold to provide a conductive matrix for charge carriers. The X-ray absorption spectral data revealed that enriched Ni<sup>3+</sup> on the surface of NCO-HNS was consequently, more active than Co to initiate the formation of NiOOH and was responsible for most redox sites acting for OH<sup>-</sup> adsorption in an alkaline solution, which was critical to enhance OER.

In summary, their observations demonstrated a strong correlation between the initialization of oxygen evolution and the formation of an active metal-oxide phase. The X-ray technique *in situ* provides a powerful tool to investigate the phase of a surface-active metal centre in electrocatalysis and can be potentially applied to probe other catalytic systems. In practical applications, solar splitting of water or artificial photosynthetic devices can be achieved through integration of a reliable catalytic system with a photovoltaic solar cell, which captures radiant energy to generate a sufficient driving force for H<sub>2</sub>/O<sub>2</sub> generation. (Reported by Yan-Gu Lin)

This report features the work of Hao-Ming Chen and his co-workers published in *Nat. Commun.* **6**, 8106 (2015) and *Adv. Energy Mater.* **5**, 1500091 (2015).

## References

1. C. W. Tung, Y. Y. Hsu, Y. P. Shen, Y. Zheng, T. S. Chan, H. S. Sheu, Y. C. Cheng, and H. M. Chen, *Nat. Commun.* **6**, 8106 (2015).
2. H. Y. Wang, Y. Y. Hsu, R. Chen, T. S. Chan, H. M. Chen, and B. Liu, *Adv. Energy Mater.* **5**, 1500091 (2015).

# Iron Titanate Kicks Off the Photogenerated Hole

Hematite is an effective photocatalyst for solar oxidation of water because of its favorable optical band gap (2.1–2.2 eV), low cost, abundance, and chemical stability in an oxidative environment. Its practical performance for solar water oxidation is, however, still poor owing to various factors such as improper band-edge position, poor conductivity, poor reaction kinetics of oxygen evolution, and short hole-diffusion length (2–4 nm). Many efforts have been made to improve the performance of hematite photoelectrodes. Ti-based treatments have also been widely used and effective methods to improve the performance of hematite photoanodes. Ti-based coating on hematite was shown to enhance effectively the performance with an obvious cathodic shift of the onset potential and an increased photocurrent. Ti-doping in hematite via various approaches such as atomic-layer deposition, deposition annealing or sol-flame synthesis, has also been widely used to improve the performance of hematite by increasing photocurrent and decreasing onset potential. Numerous mechanisms have been proposed to explain the effect of Ti-based treatments. Among them, Ti substitution of Fe in hematite (the formation of FeTiO<sub>3</sub> with Fe<sup>2+</sup>) with improved donor density has been widely reported, but the improved photoactivity of Ti incorporation in hematite could be not simply attributed to the enhanced conductivity. Meanwhile, no Fe<sup>2+</sup> signal was found in various Ti-treated hematite nanostructures. Mechanism of a Ti-based treatment was hence still an open question.

Xuhui Sun (Soochow University, China), Jun Zhong (Soochow University, China) and Shuit-Tong Lee (Soochow University, China) recorded cooperatively synchrotron-based soft X-ray absorption spectroscopy (XAS) at BL20A1 to explore the electronic structure and chemical state of hematite nanostructures before and after Ti treatment.<sup>1</sup> XAS implies the excitation of electrons from a core level to local and partial empty states, which is an effective tool to probe the electronic states of complicated materials. Two Ti treatments of hematite were used in their work; FeOOH on a FTO substrate was prepared with a hydrothermal method. One type of Ti treatment was to evaporate a TiCl<sub>4</sub> solution on the surface of FeOOH

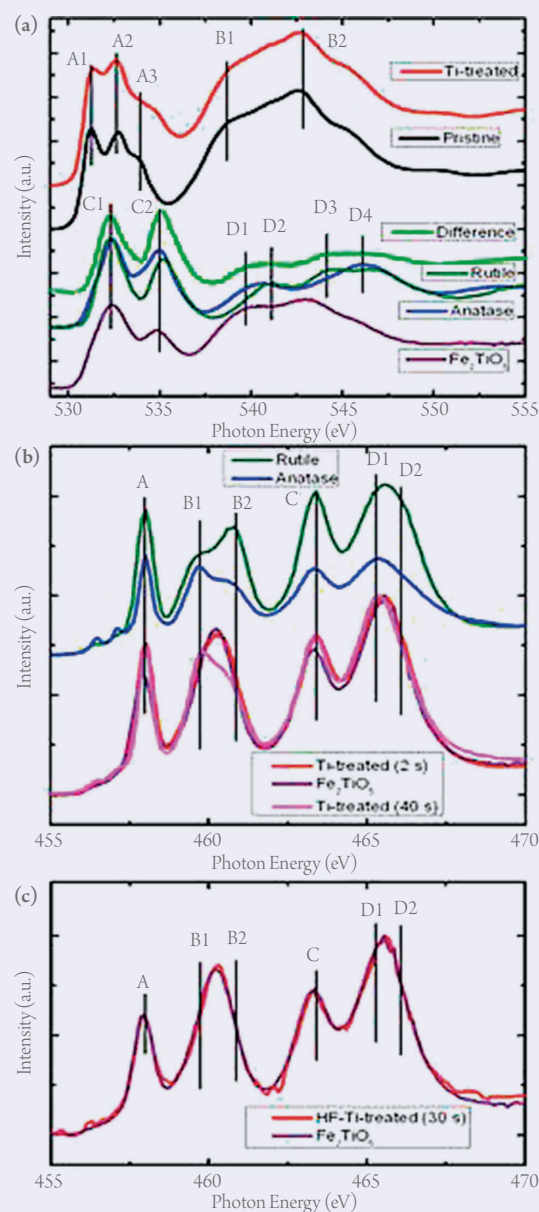


Fig. 1: (a) O K-edge XAS of pristine and Ti-treated (2 s) hematite nanostructures compared with spectra of rutile TiO<sub>2</sub>, anatase TiO<sub>2</sub>, and Fe<sub>2</sub>TiO<sub>5</sub>. The difference spectrum between the pristine and Ti-treated hematite is also shown. (b) Ti L-edge XAS of Ti-treated (2 and 40 s) hematite nanostructures compared with the spectra of rutile TiO<sub>2</sub>, anatase TiO<sub>2</sub>, and Fe<sub>2</sub>TiO<sub>5</sub>. (c) Ti L-edge XAS of HF-Ti-treated (30 s) hematite nanostructures compared with the spectrum of Fe<sub>2</sub>TiO<sub>5</sub>. [Reproduced from Ref. 1]